

Modifying Titania Using the Molten-Salt-Assisted Self-Assembly Process for Cadmium Selenide–Quantum Dot-Sensitized Photoanodes

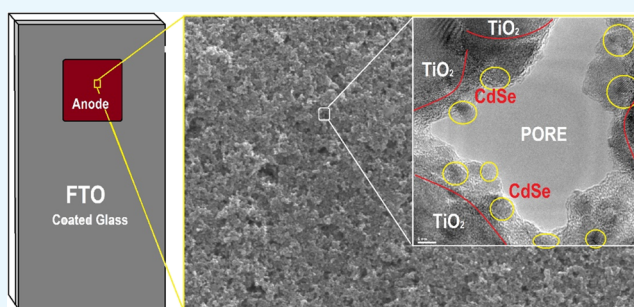
Muammer Y. Yaman,[†] Ahmet Selim Han,[†] Jayasundera Bandara,[‡] Cüneyt Karakaya,[†] and Ömer Dag^{*,†,§}

[†]Department of Chemistry and [§]UNAM-National Nanotechnology Research Center and Institute of Materials Science and Nanotechnology, Bilkent University, 06800 Ankara, Turkey

[‡]National Institute of Fundamental Studies, Hantana Road, Kandy, Central Province 20000, Sri Lanka

Supporting Information

ABSTRACT: Sensitizing titania with semiconducting quantum dots (QDs) is an important field for the development of third-generation photovoltaics. Many methods have been developed to effectively incorporate QDs over the surface of mesoporous titania, assembled from the 20–25 nm titania nanoparticles. Here, we introduce a molten-salt-assisted self-assembly (MASA) method to fabricate CdSe-modified mesoporous titania photoanodes. A mixture of ethanol, two surfactants (cetyltrimethylammonium bromide and 10-lauryl ether), silica (tetramethyl orthosilicate) or titania source ($\text{Ti}(\text{OC}_4\text{H}_9)_4$, acid (HNO_3), and cadmium nitrate solution was infiltrated into the pores of mesoporous titania (assembled using Degussa 25, P25) and immediately calcined at 450 °C to obtain mesoporous cadmium oxide–silica–titania (meso-CdO– SiO_2 –P25) or cadmium titanate–titania (meso-CdTiO₃–P25) films. The MASA process is a simple method to smoothly coat or fill the pores of titania with mesoporous CdO– SiO_2 or CdTiO₃ that can be reacted under an H_2Se atmosphere to convert cadmium species to CdSe at 100 °C. Etching of the silica films with a very dilute hydrogen fluoride solution produces mesoporous CdSe–titania (meso-CdSe–P25) electrodes. The method is flexible to adjust the CdSe/TiO₂ mole ratio over a very broad range in the films. The films were characterized at every stage of the preparation to demonstrate the effectiveness of the method. The electrodes were also tested in a simple two-electrode solar cell to demonstrate the performance of the electrodes that have a power conversion efficiency of 3.35%.



INTRODUCTION

The third-generation photovoltaic cells consisting of hybrid materials used for harvesting solar energy are a current topic of interest in the literature with a focus on meeting future energy demands.^{1–3} Quantum-dot-sensitized solar cells (QDSSCs) that consist of two different semiconductor nanoparticles are one of the promising low-cost next-generation solar cells.^{1–20} These cells consist of three components: the photoanode–electrode (quantum nanoparticles, such as CdS-, CdSe-, CdTe-, and PbS-sensitized mesoporous TiO₂), an electrolyte ($\text{S}^{2-}/\text{S}_n^{2-}$),^{12–14} and a counter electrode (CE) (usually Cu₂S nanoparticles formed over the brass plates). However, the power conversion efficiency of QDSSCs is around 4–5%, which is low compared to that of dye-sensitized solar cells.^{21–24} The reasons for the lower power conversion efficiencies include slow hole-transfer rate, back electron transfer to electrolyte, low fill factors (FFs) due to poor CE performance, limited absorption of the incident light, and so forth. Some of these issues may be addressed by properly designing the active electrode materials, sensitizer–titania, by using new synthetic approaches.

Several methods have been developed for the modification of titania by QDs, including in situ growth of quantum particles (QPs) by chemical bath deposition (CBD)⁶ or successive ionic layer adsorption and reaction (SILAR),⁷ inclusion of presynthesized QPs into the mesoscopic titania film by direct adsorption (DA),⁸ electrophoretic deposition (EPD),⁹ or using organic linkers.¹⁰ In the CBD and SILAR methods, the surface coverage of the titania nanoparticles is high compared to other methods. High coverage reduces the back electron transfer to the electrolyte. However, the synthesis of quantum nanoparticles (QPs) in a confined space (mesopores of titania films) has limitations on controlling the morphology and size of the QPs. Preparation of a decent solar-light-absorbing photoanode requires multiple loading/selenium reaction steps. During these steps, it is likely to block the mesopores that may cause a poor QP–electrolyte (redox couple) contact. The inclusion of presynthesized QPs into the mesoscopic titania film is a time-

Received: June 22, 2017

Accepted: August 11, 2017

Published: August 28, 2017

Scheme 1. Schematic Representation of Step 1, Loading of meso-P25 with Silica–Cd(II) Precursors, Followed by Calcination to Obtain meso-CdO–SiO₂–P25 and Step 2, upon H₂Se Reaction

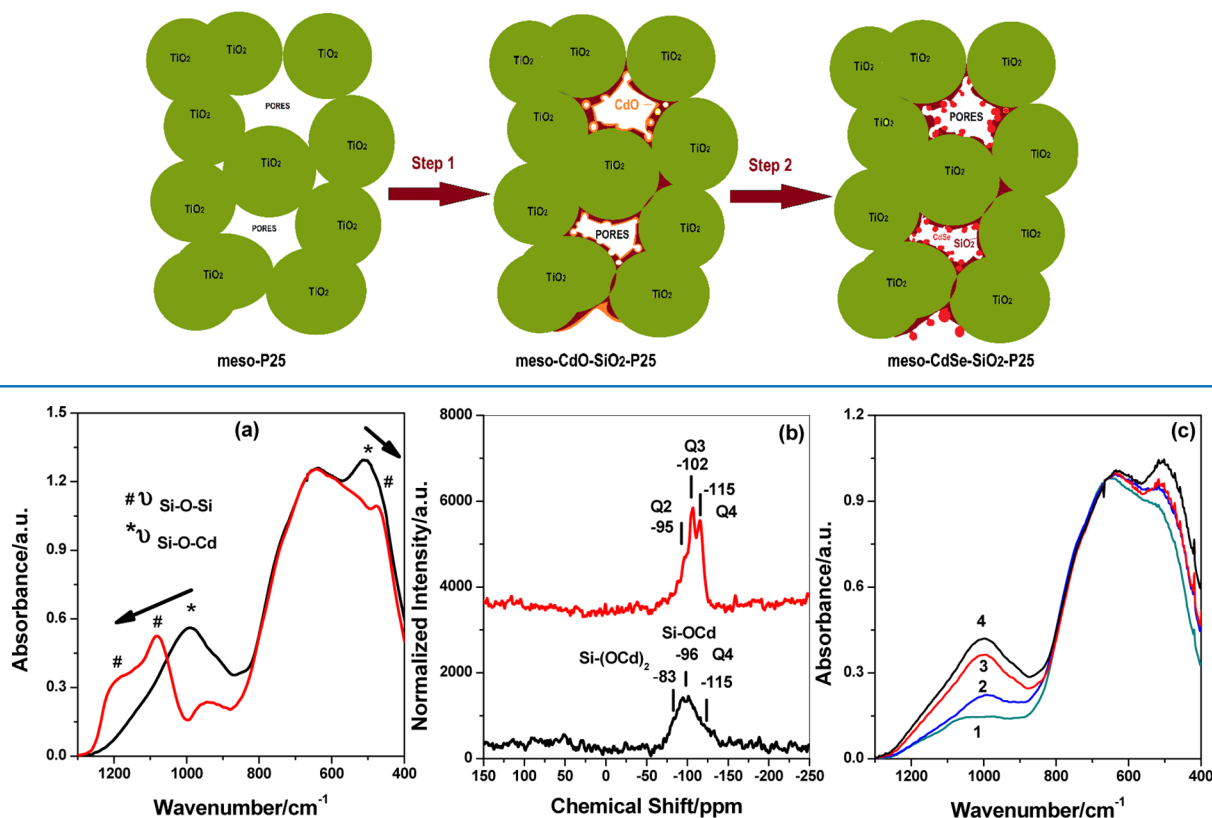


Figure 1. (a) FTIR spectra of meso-CdO–SiO₂–P25 before (black line) and after H₂Se reaction (red line), (b) ²⁹Si MAS-NMR spectra before (bottom) and after H₂Se reaction (top) of meso-CdO–SiO₂–P25, and (c) FTIR spectra of meso-CdO–SiO₂–P25 with different number of coatings.

consuming process and results in a nonuniform distribution of QPs over the titania particles. Usually, the major problem with this method is the inhomogeneous distribution of the QPs, with most being located on the solution side of the electrodes and almost none on the back of the electrode, which is the most important part of the electrode for harvesting light. The back side of the electrode has the first and most effective contact with the incoming light for the efficient conversion of light to electrical energy. EPD has also been adopted to improve the uptake of the QPs into the mesoscopic titania film. On the other hand, the surface coverage of the QPs in the DA, EPD, and organic linker is less than that of the CBD and SILAR methods.

Recently, we have developed a new self-assembly process (molten-salt-assisted self-assembly, MASA) that uses metal salts as a nonvolatile solvent and metal-ion source to incorporate a desired amount of metal oxide into mesoporous silica and metal titanate.^{25–27} The method is similar to evaporation-induced self-assembly,²⁸ where the solvent evaporates during the process, and the nonvolatile salt species and hydrolyzing/polymerizing species assemble into mesostructures as thin films, which can be calcined into mesoporous thin films. Moreover, in the MASA approach, the metal salt has dual properties: it remains as a secondary solvent to assemble hydrolyzing/polymerizing species into mesostructures by remaining a liquid between the surfactant and solidified pore walls, and later, upon calcination, it can be deposited as a thin layer of metal oxide over the silica wall or as a metal titanate pore wall. This is a very

effective way of incorporating metal ions into the mesopores as a reactive metal oxide with a very high density, over a 100% metal oxide/silica mole ratio.²⁶ The MASA process also eliminates the formation of acids of the counter anion (usually nitrate or chloride) of the salt, used as a metal-ion source, in the H₂S or H₂Se reactions to convert the metal ions into metal sulfide or metal selenide QPs.²⁹

Here, we introduce a new method of modifying mesoporous titania with QPs, which can be synthesized inside mesopores. The 20–25 nm titania particles (Degussa 25, P25) are first dispersed into ethanol and coated over a glass or fluorine-doped tin oxide (FTO) substrate. The ingredients of the silica–metal oxide or metal titanate precursors are then spin-coated over this film, which can be calcined to obtain mesoporous silica–cadmium oxide or metal titanate incorporated into the mesoporous titania films. Exposing these films to an H₂Se atmosphere produces CdSe-sensitized mesoporous films.

RESULTS AND DISCUSSION

Synthesis of the meso-CdO–SiO₂–P25 and meso-CdSe–SiO₂–P25 Films. The titania (P25) film (meso-P25) that provides mesopores (5–50 nm) for the infiltration of the silica precursor solution was prepared as described in the [Experimental Section](#). Then, a clear ethanol solution of cadmium nitrate tetrahydrate ([Cd(H₂O)₄](NO₃)₂), tetramethyl orthosilicate (TMOS), 10-lauryl ether (C₁₂E₁₀), cetyltrimethylammonium bromide (CTAB), and nitric acid is infiltrated into the pores by dropping, followed by spin coating

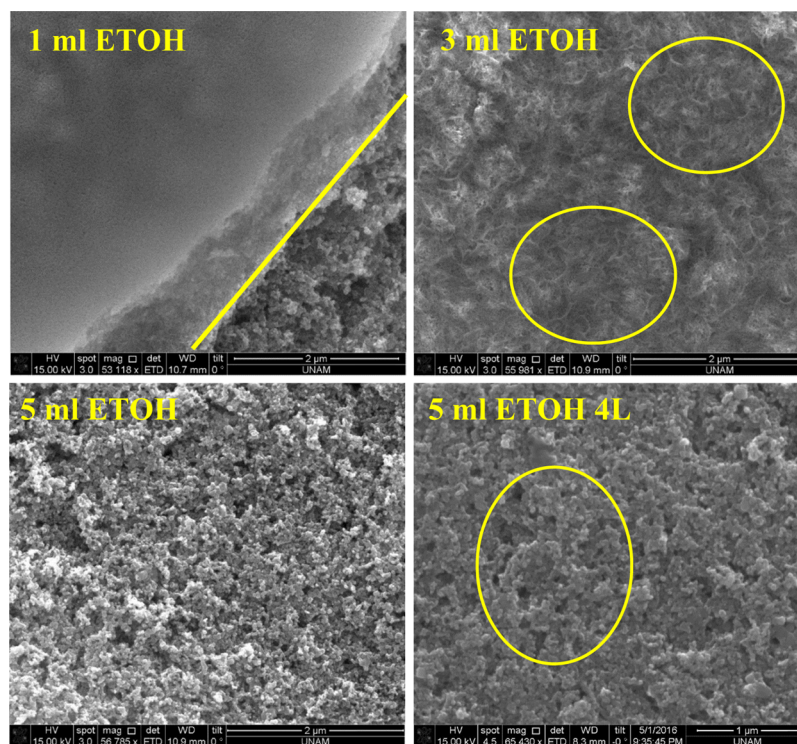


Figure 2. SEM images of the meso-CdO-SiO₂-P25, prepared using solutions with different amounts of ethanol (1, 3, and 5 mL of ethanol single coatings) and four-layer coating (4L) using the solution prepared in 5 mL of ethanol, as marked over the images.

to remove any unfiltered solution from the top of the film. It is also likely that upon evaporation of the volatile solvent (ethanol) and further condensation of the silica species, its volume shrinks and causes further sucking of this upper gel-like layer into the pores through capillary forces. Therefore, under certain conditions, there is no CdO-SiO₂ film formation over the meso-P25 films upon calcination. The infiltrated solution slowly goes into the gel phase and then solidifies over time (see ref 22 for details) in the mesopores, Scheme 1. The calcination of this film produces a CdO-silica-filled mesoporous titania, denoted as meso-CdO-SiO₂-P25.

The Fourier transform infrared (FTIR) spectra of the calcined samples display peak(s) because of ν -Si-O-Cd stretching mode at around 990 cm⁻¹, as shown in Figure 1a. No CdSiO₃ formation was observed in the samples, indicating that the silica species are acting as a blocking layer (see later in the titania system) over the titania surface; infrared spectra of CdSiO₃ display sharp characteristic peaks at 603, 707, 834, and 929 cm⁻¹.^{26,30} Also, ²⁹Si MAS-NMR spectra, in Figure 1b, support the above-proposed structure that one can observe Q₄ sites (Si(OSi)₄, at -115 ppm) and Si(OSi)_{4-x}(OCd)_x sites (where x is 1 and 2, observed at -96 and -83 ppm, respectively).³¹ The reaction between the meso-CdO-SiO₂ and H₂Se produces CdSe-SiO₂ over the surface of P25. Both FTIR and ²⁹Si MAS-NMR spectra display only pure silica-related peaks (peak at 1082 and shoulder at 1190 cm⁻¹) in the FTIR spectra and Q₂, Q₃, and Q₄ peaks³¹ in the ²⁹Si MAS-NMR spectra; the Q₂ and Q₃ sites form upon the reaction of H₂Se with the Si(OSi)₃(OCd) and Si(OSi)₂(OCd)₂ interfaces, respectively, see Figure 1b, indicating that all Cd(II) species are reacted to form CdSe. This is an important observation in understanding the formation process. Figures 1c and S1 show the FTIR spectra of the sample upon a consecutive loading and loading using different amounts of ethanol solutions,

respectively. However, both sets of samples have very similar spectral changes with increasing loading (multiple loading is a consecutive process of loading/calcination) or single loading using less viscous ethanol solution (the same ingredient composition in 1, 3, 5, and 10 mL of ethanol). Gradual increase of the ν -Si-O-Cd peak at 990 cm⁻¹ shows that loading is quantitative and can be controlled either by multiple loading or by using concentrated MASA solutions (see Figures 1 and S1). Further analysis is needed to differentiate between these two sets of samples because the samples display very low solar efficiency upon loading using less viscous solutions; on the other hand, multiple loading enhances the efficiency (see later).

To elucidate the nature of meso-CdO-SiO₂ over the surface of meso-P25, the samples prepared using 1, 3, 5, and 10 mL of ethanol solutions were investigated using the scanning electron microscopy (SEM) imaging, sorption, and spectroscopic techniques. Figure 2 shows a set of SEM images displaying a thin layer of meso-CdO-SiO₂ formation, when the ethanol amount in the clear solution is less than 3 mL. However, the meso-CdO-SiO₂ film over the electrode surface diminishes with an increasing ethanol amount in the precursor mixture and completely disappears at around 5 mL of ethanol (see Figure 2). Also note that the ethanol amount is relative, and if one doubles the ingredients (salt and surfactant species) in the solution, the ethanol amount should be doubled to get a similar viscosity. Both solutions prepared using 1 and 3 mL of ethanol show meso-CdO-SiO₂ film layers over the titania films (meso-P25), as marked on the images (Figure 2). However, when the ethanol amount is increased to 5 mL and above, no meso-CdO-SiO₂ film formation was observed over the electrodes. However, infiltration of the dilute solutions results a low CdO-SiO₂ loading; therefore, it may be necessary to load the films multiple times to reach to a desired sensitizer concentration.

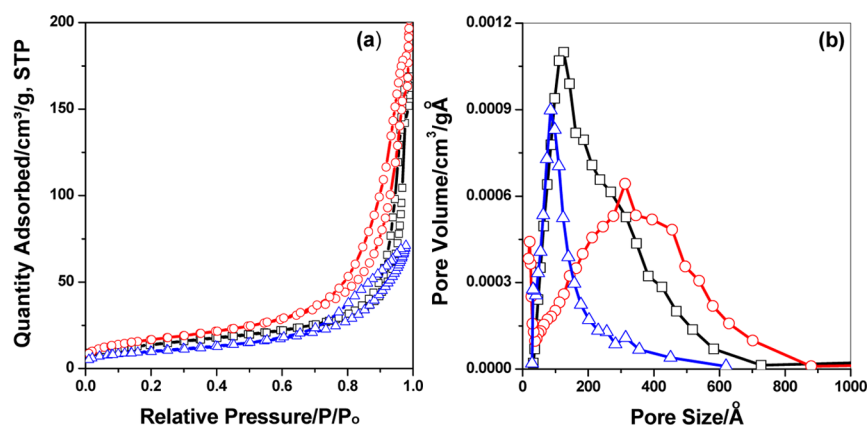


Figure 3. N_2 (77.4 K) sorption measurement (a) isotherm and (b) Barrett–Joyner–Halenda pore size distribution plot of TiO_2 nanoparticles before loading with ethanol (black line), loading with less ethanol (red line), and four times loading with ethanol (blue line).

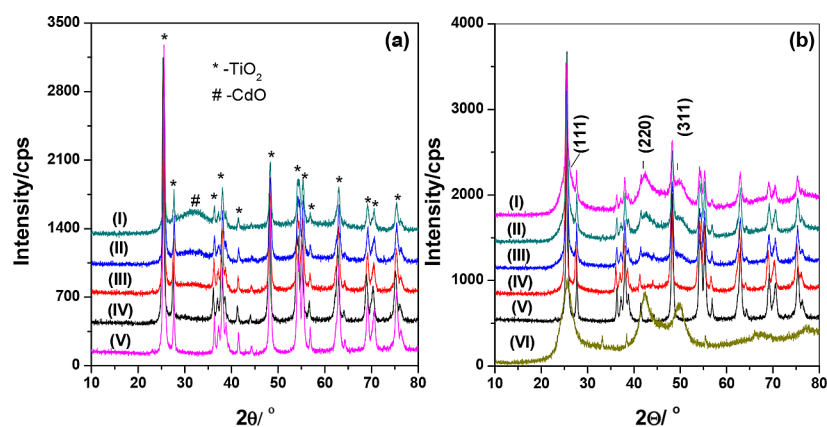


Figure 4. XRD pattern of meso- $CdO-SiO_2-P25$ prepared using different amounts of ethanol solutions (a) before H_2Se reaction and (b) after H_2Se reaction (indexes correspond to the $CdSe$ nanoparticles). Samples were prepared from (I) 1, (II) 2.5, (III) 5, (IV) 10 mL of ethanol solutions, (V) meso- $P25$, and (VI) meso- $CdSe-SiO_2$ film.

Notice also that the evaporation of ethanol from the coated mixture leaves the nonvolatile species, as a gel, in the mesopores of meso- $P25$; therefore, the salt/silica and salt/surfactant mole ratios are preserved; the only difference among the samples, prepared using different amounts of ethanol, is the total amount of gel formed upon the evaporation of ethanol in and over the titania films. There is a distinct morphology difference among the electrodes that have meso- $CdO-SiO_2$ film coverage; the formation of a meso- $CdO-SiO_2$ film over the electrode surface is detrimental for the solar cell performance due to no solar performance of the meso- $CdSe-SiO_2$ film. Only meso- $CdO-SiO_2$ species, useful in solar cell activity, are the ones in the pores of meso- $P25$, where the titania nanoparticles are uniformly coated with a very thin layer of $CdO-SiO_2$. We also checked the SEM images of the samples, prepared using dilute precursor solutions over multiple steps (see Figure S2). Each loading step involves infiltration followed by calcination at 450 °C for 1 h. The samples loaded two, three, and four times were analyzed, and after four times loading, meso- $CdO-SiO_2$ film layers over the titania films were observed (see Figure S2). One can make multiple loading for a desired amount of meso- $CdO-SiO_2$ coating over the titania particles without any film formation. We also collected energy-dispersive system (EDS) data along the thickness axis of two different samples, loaded using 1 and 5 mL of ethanol solutions and calcined at 450 °C, to show the homogeneous coating of the internal surface of the meso- $P25$

film. Figure S3 shows the cross-sectional SEM images and the elemental (Si, Cd, and Ti) analysis along the cross section (line scan along the thickness axis of the films). The film formation over the meso- $P25$ film is clearly visible in both SEM image and EDS data (Figure S3) in the case of 1 mL of ethanol. The meso- $CdO-SiO_2-P25$ film, obtained from 5 mL of ethanol solutions, contains homogeneous elemental (Si, Cd, and Ti) distribution throughout the film.

The N_2 sorption isotherms of the films show type IV isotherms with a hysteresis, showing that they are all mesoporous before and after loading (see Figure 3). The samples, loaded using concentrated solutions (1–3 mL of ethanol) or four times loaded using dilute solutions (in 5 mL of ethanol), display a much narrower pore size distribution at around the 2–3 nm region in the pore size distribution plots (Figure S4). Notice that the smaller pores, due to the meso- $CdO-SiO_2$ film layer, increase with increased loading. However, the samples prepared using dilute solutions and multiple loadings display a gradual diminishing of the pores in the titania film domains without smaller pores (see isotherms and pore size distribution plots in Figure S4) also indicating no film formation over the meso- $P25$ film.

We also collected the X-ray diffraction (XRD) patterns of the above samples and observed that the $CdO-SiO_2$ domains are mesoporous with low or no crystallinity (see Figure 4). The broad feature at around 30°, 2θ , gradually increases with reducing ethanol in the clear solution and with multiple

coatings. This feature arises from the (110) and (111) planes of the ultrathin CdO (around 1.6 nm) layer over the silica (see ref 26 for details). The sharp lines originated from P25 titania³² nanoparticles, consisting of 80% anatase and 20% rutile phase. However, upon reaction under an H₂Se gas, stronger and broad lines due to (111), (220), and (311) planes of the nanocrystalline zinc-blended CdSe appear at 25.4°, 41.9°, and 49.5°, 2 θ , respectively.³³ The CdSe nanoparticles are on average 3–4 nm, calculated using the Scherrer equation. Notice also that with decreasing ethanol, the only change is in the intensity of the CdSe diffraction lines that gradually increases with a decreasing ethanol amount in the original solution. Therefore, it can be concluded that the CdSe nanoparticles in pores (meso-CdSe–SiO₂–P25) and in the meso-CdSe–SiO₂ film over titania have a similar origin. Figure 4 also shows the XRD pattern of meso-CdSe–SiO₂ for comparison purpose and meso-P25 as a reference.

The meso-CdO–SiO₂–P25 and meso-CdSe–SiO₂–P25 films were further analyzed using transmittance electron microscopy (TEM) imaging. Figures 5 and S5 display the

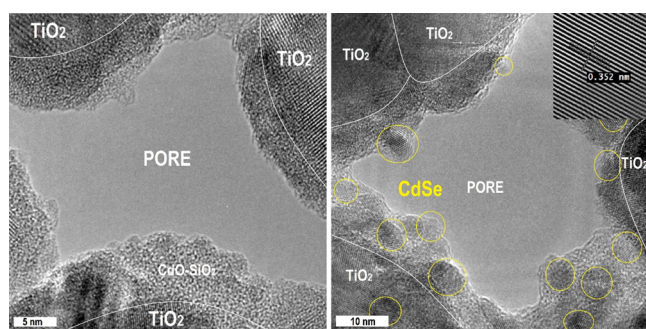


Figure 5. TEM images of meso-CdO–SiO₂–P25 (left, scale bar 5 nm) and meso-CdSe–SiO₂–P25 films (right, scale bar 10 nm, CdSe particles are in yellow circles). Inset is FFT and inverse FFT of the selected area from a CdSe particle.

TEM images of meso-CdO–SiO₂–P25 and meso-CdSe–SiO₂–P25 films. Clearly, one can distinguish both mesoporous CdO–SiO₂ domains over the spherical nanocrystalline titania (P25) and 3–4 nm CdSe nanocrystals (consistent with the XRD and N₂ sorption data) in the films before and after H₂Se reaction, respectively. A detailed analysis of the high-resolution TEM image of meso-CdSe–SiO₂–P25 by fast Fourier transform (FFT) and inverse FFT of the selected area reveals lattice fringes with a spacing of around 0.352 nm that originate from the (111) plane of the CdSe particle (see Figure 5). From the high-resolution image, the distinguished specific lattice planes of the titania, cadmium oxide, and cadmium selenide accord with the results, obtained from the XRD data.

Synthesis of meso-CdTiO₃–P25 and meso-CdSe–TiO₂–P25 Films. The MASA process has also been employed to coat the films of the titania nanoparticle (meso-P25) by CdTiO₃, by replacing the silica source with a titania source. The clear solution that contains two surfactants (C₁₂EO₁₀ and CTAB), two solvents (ethanol and [Cd(H₂O)₄](NO₃)₂), acid, and titanium tetrabutoxide is infiltrated into the pores of a prefabricated titania film and calcined immediately at 450 °C to convert the precursors into mesoporous CdTiO₃.²⁵ The H₂Se reaction of meso-CdTiO₃ has produced CdSe and TiO₂ nanoparticles over the films of titania (P25) nanoparticles.²⁵ Because the CdTiO₃-coated meso-P25 (meso-CdTiO₃–P25)

produces bared TiO₂ upon reaction under an H₂Se atmosphere, it is important to control the reaction atmosphere.²⁵ In the presence of oxygen/water, a bared titania surface promotes Se(0) formation and results a dark red color (due to Se particles), which may be misleading. The selenium formation can be monitored using Raman spectroscopy. The Raman spectra (Figure 6) display a peak at 250 cm⁻¹ because of the Se metal,³⁴ in addition to a peak at around 200 cm⁻¹ and its overtone at around 400 cm⁻¹ (overlap with the titania peak) because of CdSe nanoparticles.³⁵ The other intense peaks at 150, 196, 393, 511, and 632 cm⁻¹ are due to the anatase phase of titania (P25 particles).³⁶ Also notice that the CdSe signals are much more intense in the silica samples, compared to those in the titania samples, indicating a lower reactivity of CdTiO₃. However, the reactions carried under vacuum conditions or N₂ atmosphere reduce the selenium formation to below the Raman detection limits.

Moreover, the H₂Se reaction of meso-CdTiO₃–P25 is less reactive compared to that of meso-CdO–SiO₂–P25 samples. To demonstrate this, we also prepared thin films of both meso-CdO–SiO₂ and meso-CdTiO₃ without P25 nanoparticles, and both reactions were monitored using Raman spectroscopy. The CdSe signals are much more intense in the silica samples without a selenium signal (Figure 6a,b). For a complete reaction between meso-CdTiO₃ and H₂Se, the samples must be kept under an H₂Se atmosphere at higher temperatures and longer durations, which may cause other problems. The presence of air in the H₂Se reaction media enhances the selenium formation in the meso-CdTiO₃–P25 system. To elucidate the origin of the side reaction, the H₂Se reaction over a Cd(II) free sample (bared titania film) was also carried out, and it was discovered that the only product is Se(0) (Figure S6). Therefore, it is reasonable to conclude that the bared titania surface promotes the Se(0) formation through converting O₂ to water. Also note that the meso-CdTiO₃ produces bared titania²⁵ and water during the H₂Se reaction as side products and therefore promotes the Se(0) formation. However, the Se(0) species can be effectively removed by washing the samples using a Na₂S solution before or during solar cell measurements, where the solar cell measurements are carried out using a Na₂S/S₈ solution and also by sublimation under vacuum at around 200 °C.

Response of meso-CdSe–SiO₂–P25 and meso-CdSe–TiO₂–P25 Samples to Green Laser and Solar Cell Performance. We discovered that the final products are very sensitive to green laser exposure under the Raman spectroscopy; both meso-CdSe–SiO₂–P25 and meso-CdSe–TiO₂–P25 samples undergo slow decomposition that can be monitored using the CdSe Raman signal. Both silica and titania samples, coated over an FTO substrate or any conducting substrate, give the same response. However, the decomposition is not observed if the substrate is a non-conducting material such as glass. This behavior is important to demonstrate the response of the photoanode (meso-CdSe–SiO₂–P25 and meso-CdSe–TiO₂–P25) to the light. The excited CdSe loses its electrons to titania and then to the conducting substrate; therefore, it undergoes oxidation and as a result decomposition. The decomposition product is currently unknown, but the CdSe Raman signal at around 200 cm⁻¹ decays over time and does not recover upon removing the laser beam, indicating an irreversible process (see Figure 6). The Raman intensity of both samples was normalized to titania signal³⁶ at around 150 cm⁻¹ to evaluate both the decay behavior

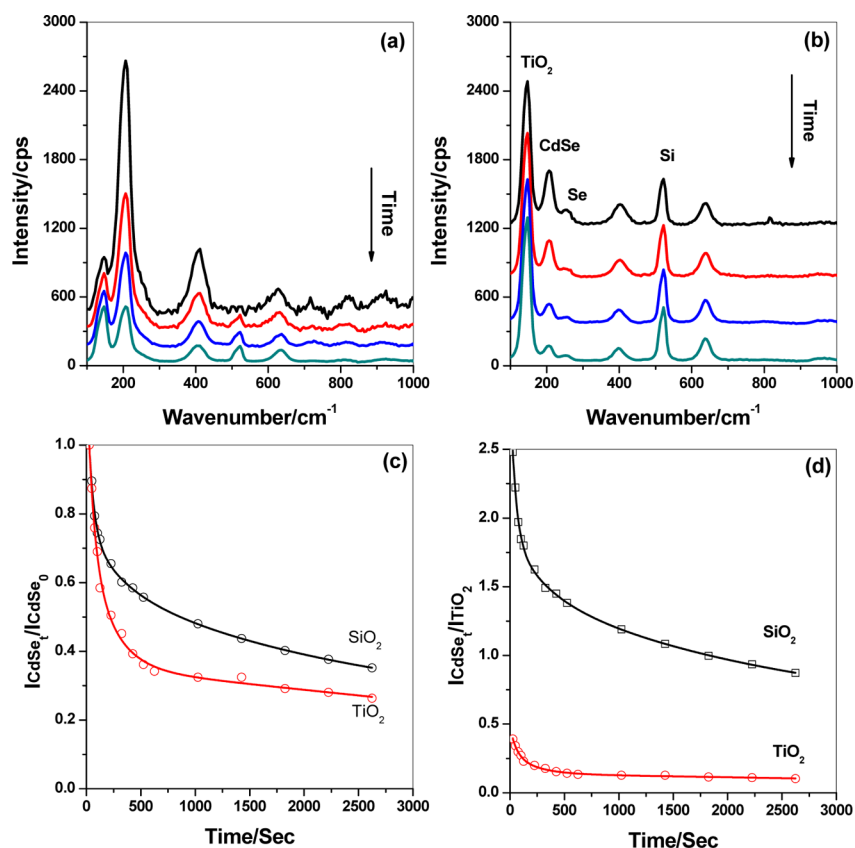


Figure 6. Raman spectra of (a) meso-CdSe–SiO₂–P25 and (b) meso-CdSe–TiO₂–P25 over laser exposure time and intensity ratio of (c) (CdSe)_t/I(CdSe)₀ and (d) (CdSe)_t/I(TiO₂) over time.

and the relative amount of CdSe produced in both silica and titania samples. Figure 6c,d shows the normalized decay plots of intensity ratios of $I(\text{CdSe})_t/I(\text{CdSe})_0$ (t any time, 0 at time zero) and $I(\text{CdSe})_t/I(\text{TiO}_2)$ over time. Both meso-CdSe–SiO₂–P25 and meso-CdSe–TiO₂–P25 show similar decay curves, but the normalized decay curves show that the silica sample decays more quickly. This indicates that the silica layer over the titania does not affect the electron flow from the excited CdSe to titania through a silica layer. Note also that the CdSe nanoparticles are flakelike in the silica²⁶ and spherical in the titania²⁵ systems. Therefore, the fast decay may be due to the amount of CdSe and its flakelike morphology in the silica system.

To measure the solar performances of both types of anode electrodes, the QDSSC was assembled by sandwiching a standard S²⁻/S₈ electrolyte between the anode constructed as described above and the Cu₂S cathode electrode, produced by activating the brass plate in acid and Na₂S solution. Typical I – V curves under 1 sun condition of silica-based cells are shown in Figure 7, and the cell characteristics of the electrodes fabricated under different preparation conditions are tabulated in Table 1. Most investigations have been carried out using thin photoanodes that are prepared by coating a dispersed slurry of P25 in excess ethanol. This ensures to produce uniform and thin films (typical film thickness of 1 μm) with relatively lower cell efficiencies. However, when increasing the meso-P25 film thickness using the doctor blade method, the efficiencies of the cells could be increased. We have found out that both silica- and titania-based anodes show similar cell characteristics with a percent FF of 50–60 and open-circuit voltage (V_{oc}) of 0.5–0.6 V. However, the maximum efficiency was detected from the

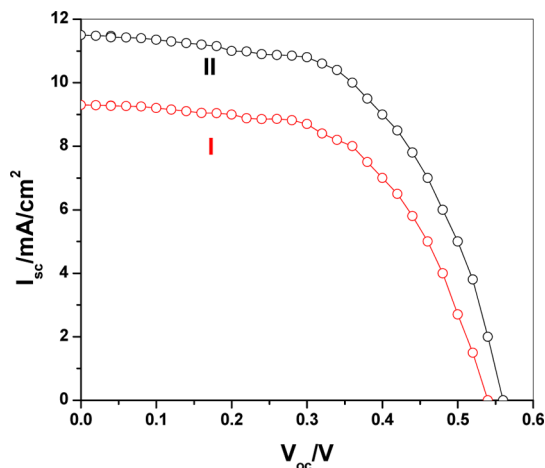


Figure 7. I – V curves of meso-CdSe–SiO₂–P25 single (I) and double (II) loading.

Table 1. Solar Cell Performances of Various Samples (1L Single and 2L Double Coatings)

samples	I_{sc} (mA)	V_{oc} (V)	FF	η %
meso-CdSe–TiO ₂ –P25	6.02	0.52	0.52	1.30
meso-CdSe–SiO ₂ –P25	6.60	0.48	0.53	1.40
meso-CdSe–P25 (etched)	7.10	0.50	0.49	1.46
meso-Cd _x Mn _{1-x} Se–TiO ₂ –P25	8.09	0.54	0.51	1.84
meso-Cd _x Se/Mn _{1-x} Se–SiO ₂ –P25	8.25	0.56	0.47	1.79
meso-CdSe–SiO ₂ –P25 (1L)	9.30	0.54	0.54	2.70
meso-CdSe–SiO ₂ –P25 (2L)	11.50	0.55	0.52	3.30

silica samples with a % FF of 60 and V_{oc} of 0.6 V, and a short current (J_{sc}) of 10 mA has been recorded using relatively thicker films with a double loading. Further treatments, such as removing silica layer by dilute hydrogen fluoride (HF), can effectively remove silica,²⁶ but the resulting sample does not have a better solar cell performance. It is likely that removing the silica layer between the titania domains and CdSe nanoparticles breaks the contact between the titania and the sensitizers and creates more bared titania surfaces. Therefore, further treatments are necessary to overcome the damage of HF treatment to improve the cell performance.

The efficiencies of the cells can be further optimized by introducing Mn(II) into the CdSe sensitizer using the MASA process. The MASA process is a quite flexible method to introduce Mn(II) and other metals into the media that may also boost the solar performance of the cells.¹⁰ We observed that the cell performance can be improved by 40% upon modifying the samples by introducing about 13% Mn(II) into the CdTiO₃ samples (see Table 1). However, the improvement in the silica samples was limited to around 13% for the same Mn(II)/Cd(II) ratio. Note that the oxides in the titania systems are metal titanates,^{25,27} in which both CdTiO₃ and MnTiO₃ form the same structure; therefore, the titania system is likely to form a solid solution of Cd_{1-x}Mn_xTiO₃, where the H₂Se reaction can effectively produce a solid solution of Cd_{1-x}Mn_xSe as a sensitizer. However, in the silica system, it is not possible to form Cd_{1-x}Mn_xO because both oxides have different crystal structures and do not form a solid solution. Therefore, the H₂Se reaction produces a solid solution with smaller Mn(II)/Cd(II) ratio in the Cd_{1-x}Mn_xSe nanoparticles, and the major products are likely to be individual metal selenides, CdSe and MnSe. As a result, the addition of Mn(II) in the titania system enhances the cell performance more than that in the silica system. Even though, this is the case, the Mn(II) produced through the MASA process improves the solar cell performances of both systems and the cells produced by our method should be further investigated by introducing current improvements in the cathode side.

CONCLUSIONS

The MASA process has been used for the assembly of the CdSe-sensitized titania-based photoanode for QDSSCs. The process starts as a clear solution of a polymerizing agent (silica, TMOS, or titania, Ti(OBu)₄), surfactants (C₁₂E₁₀ and CTAB), acid, and salt. The polymerizing agent ensures the formation of nano-CdO or nano-CdTiO₃ for the formation of nano-CdSe in the pores of meso-P25 upon H₂Se reaction. The MASA is an effective process to uniformly coat the internal surface of the titania films (prepared using P25) to produce meso-CdO–SiO₂–P25 and meso-CdTiO₃–P25 films that can be converted into CdSe–SiO₂–P25 and CdSe–TiO₂–P25 under an N₂/H₂Se atmosphere. The viscosity of the clear MASA solution has a critical importance in the effective coating of the internal surface of the titania films; with an incorrect viscosity, the process may instead produce a blocking thin layer of mesoporous CdO–SiO₂ or CdTiO₃ over the titania film. The H₂Se and meso-CdO–SiO₂–P25 reaction is a complete and clean process, compared to the same reaction of meso-CdTiO₃–TiO₂–P25.

A typical cell can be fabricated with a solar cell efficiency of around 3.3% but can be further improved by introducing Mn(II) into the sensitizer. Incorporation of Mn(II) is more effective in the titania system than the silica system because of

the formation of a solid-solution-type precursor in the titania system, rather than individual oxides of Mn(II) and Cd(II) in silica. However, the cells, prepared using silica and titania precursors, display similar solar cell performances; even though silica is an insulating material, its high reactivity and morphology difference provide a slightly better performance as an anode in the solar cell. Further improvements can be achieved by further modifying the anode by multiple coatings and doping. The MASA process, used in this work, is a very flexible method and can be used to add different metal impurities to the photoanode films and to the QDSSCs.

EXPERIMENTAL SECTION

Preparation of Mesoporous Titania Films (meso-P25).

P25 (1.5 g, titania, Aldrich grade) was dispersed into a 5 mL of ethanol by stirring, and then the mixture was sonicated for 30 min. Titanium tetrabutoxide (Ti(BuO)₄, 0.25 mL) and concentrated nitric acid (0.5 g, 65%) were added into the dispersion and stirred for another 5 min. Half of the FTO glass was isolated by using a scotch tape. Then, the FTO glass was spin-coated using the above solution at 2000 rpm. The tape was removed, and then the sample was calcined at 450 °C for 15 min and was denoted as meso-P25.

The thicker films were obtained by using a thicker dispersion. The dispersion was prepared by using a paste: 0.2 g of P25 was mixed with 12 drops of acetic acid, 0.6 mL of ethanol, 0.6 mL of water, and 1 drop of Triton-100 in a mortar and grounded well until it becomes a paste. Then, the paste was spread over half of the FTO glass, and then the sample was annealed at 450 °C for 1 h and was denoted as meso-P25.

Synthesis of Mesoporous Cadmium Oxide–silica–titania Films (meso-CdO–SiO₂–P25). C₁₂EO₁₀ (0.500 g, 0.8 mmol) and CTAB (0.291 g, 0.8 mmol) were dissolved in a 5 mL of ethanol (the same compositions were also prepared in 1, 3, and 10 mL of ethanol). Then, [Cd(H₂O)₄](NO₃)₂ (1.970 g, 6.4 mmol) and TMOS (0.85 g, 5.6 mmol) were added to the above solution, and the solution was stirred for 5 min. The meso-P25 film was located over the spin coater, and the above solution was put as drops (to ensure that the solution is really soaked into the film) and was spin-coated at 1000 rpm for 30 s. Immediately after spin coating, the film was placed in an oven at 65 °C and the sample was calcined up to 450 °C with a 1°/min increments.

Synthesis of Mesoporous Mn(II)-Doped Cadmium Oxide–Silica–Titania Films. The above procedure was used for the synthesis of Mn(II)-doped films with some modifications. [Mn(H₂O)₄](NO₃)₂ (0.21 g, 0.83 mmol) and [Cd(H₂O)₄](NO₃)₂ (1.715 g, 5.57 mmol) were used as salts for 13% Mn(II) doping. For lower dopings, Mn(II) in the clear solutions was reduced accordingly.

Synthesis of Mesoporous Cadmium Titanate–Titania Films (meso-CdTiO₃–P25). C₁₂EO₁₀ (0.500 g, 0.8 mmol) and CTAB (0.291 g, 0.8 mmol) were dissolved in a 5 mL of ethanol. Then, [Cd(H₂O)₄](NO₃)₂ (1.970 g, 6.4 mmol) and Ti(BuO)₄ (1.91 g, 5.6 mmol) were added to the above solution, and the solution was stirred for 5 min. The meso-P25 film was located over the spin coater, and the above solution was put as drops (to ensure that the solution is really soaked into the film) and was spin-coated at 1000 rpm for 30 s. Immediately after spin coating, the film was placed in an oven at 65 °C and the sample was calcined up to 450 °C with a 1°/min increments.

Synthesis of Mesoporous Mn(II)-Doped Cadmium Titanate–Titania Films. The above procedure was used for

the synthesis of Mn(II)-doped films with some modifications. $[\text{Mn}(\text{H}_2\text{O})_4](\text{NO}_3)_2$ (0.21 g, 0.83 mmol) and $[\text{Cd}(\text{H}_2\text{O})_4](\text{NO}_3)_2$ (1.715 g, 5.57 mmol) were used as salts for 13% Mn(II) doping. For lower dopings, Mn(II) in the clear solutions was reduced accordingly.

Synthesis of Mesoporous Cadmium Selenide–Silica–Titania (meso-CdSe–SiO₂–P25) Films and Mesoporous Cadmium Selenide–Titania (meso-CdSe–TiO₂–P25) Films. The calcined meso-CdO–SiO₂–P25 or meso-CdTiO₃–P25 was inserted into a vacuum chamber designed for an H₂Se reaction, and the chamber was evacuated for a few minutes before exposing the sample to the H₂Se atmosphere. About 100 Torr of H₂Se was added, and the reaction was carried out for 30 min at 100 °C. The chamber was evacuated by pumping the unreacted H₂Se and water (side product) first over CdO-loaded silica and then into the atmosphere through the fume hood, and the films were removed for analysis and further treatments.

Preparation of the CE. The CE and the electrolyte solution were prepared as in the literature.¹² The electrolyte solution containing 2 M Na₂S·9H₂O and 2 M S was prepared in 10 mL of water. The CE was prepared by etching brass with 1 M HCl for 5 min at 70 °C and reacted with 0.1 M Na₂S·9H₂O solution.

ZnS Treatments Prior to Solar Performance Measurement of the Electrode. The photoanode electrode was dipped into 0.1 M Zn(II) solution (prepared by $[\text{Zn}(\text{H}_2\text{O})_6](\text{NO}_3)_2$) for 30 s, rinsed with ethanol, and then dipped into 0.1 M S²⁻ solution (prepared by Na₂S·9H₂O) for 30 s. This step was repeated three times to ensure that all the pore surfaces are covered with ZnS nanoparticles.

Installation of the QDSSC. The above two electrodes (meso-CdSe–SiO₂–P25 or meso-CdSe–P25 as photoanode working electrode) and modified brass (CE) were sandwiched using a spacer (Parafilm) and the above Na₂S/S₈ aqueous solution as the electrolyte in between and clamped with a paper clip.

Instrumentation. The FTIR spectra were recorded using a Bruker TENSOR 27 model FTIR spectrometer. A Digi Tech TM DLATGS detector with a resolution of 4.0 cm⁻¹ in the 400–4000 cm⁻¹ range was used. The spectra were recorded using the samples coated on silicon wafers or using dry KBr pallets. The micro-Raman spectra were recorded on a LabRAM confocal Raman microscope with a 300 mm focal length. The spectrometer was equipped with a Ventus LP 532 at 50 mW, diode-pumped solid-state laser operator at 20 mW, with a polarization ratio of 100:1, a wavelength of 532.1 nm, and a 1024 × 256 element charge coupled device camera. The signal collected was transmitted via a fiber optic cable into a spectrometer with 600 g/mm grating. The Raman spectra were collected by manually placing the probe tip on the desired point of the sample over the glass or silicon wafer. The XRD patterns were recorded on a Rigaku MiniFlex diffractometer using a high-power Cu K α source operating at 30 kV/15 mA. The SEM images and the EDS data were obtained using a FEI Quanta 200 FEG ESEM instrument and a Zeiss EVO-40 SEM instrument operating at 15 kV, respectively, and a Bruker AXS XFlash detector 4010 attached to the same microscope using the same samples. TEM images were recorded on FEI Tecnai G2 F30 and JEOL JEM 2100F instruments at an operating voltage of 200 kV. The calcined film samples were scraped and grounded in a mortar with 5 mL of ethanol and dispersed using sonication for 5 min. One drop of the dispersed ethanol

solution was put on a TEM grid and dried under a powerful lamp. The N₂ (77.4 K) sorption measurements were performed with a TriStar 3000 automated gas adsorption analyzer (MicroMetrics) in a relative pressure range, P/P_0 , from 0.01 to 0.99. To provide high accuracy and precision in the determination of P/P_0 , the saturation pressure P_0 was measured over 120 min intervals. The powder samples of the films, obtained by scraping a few glass slides, were dehydrated under a ($\sim 10^{-2}$ Torr) vacuum for 3 h at 250 °C before measuring to remove adsorbed water and volatile species in the pores. A Bruker Superconducting FT-NMR spectrometer Advance TM 300 MHz WB spectrometer with a 7 mm double-channel Bruker probehead was used at room temperature for ²⁹Si MAS-NMR spectra. The solar performance measurements were made by using an AM 1.5 solar simulator equipped with a 300 W xenon lamp (model no. 81172, Oriel). The light intensity was set to 1000 W/m² by using a reference Si photodiode. The I – V curves were obtained by applying an external bias to the cell and measuring the generated photocurrent using a Keithley model 2400 digital source meter.

■ ASSOCIATED CONTENT

📄 Supporting Information

The Supporting Information is available free of charge on the ACS Publications website at DOI: 10.1021/acsomega.7b00839.

More SEM and TEM images, XRD patterns, N₂ sorption data, Raman spectra, and solar cell performance data (PDF)

■ AUTHOR INFORMATION

Corresponding Author

*E-mail: dag@fen.bilkent.edu.tr (Ö.D.).

ORCID

Ömer Dag: 0000-0002-1129-3246

Author Contributions

The manuscript was written through contributions from all authors. All authors have given approval to the final version of the manuscript.

Notes

The authors declare no competing financial interest.

■ ACKNOWLEDGMENTS

We thank the Scientific and Technological Research Council of Turkey (TÜBİTAK) under project number 112T407 for the financial support. M.Y.Y. thanks TÜBİTAK for the graduate scholarship (2210). J.B. thanks TÜBİTAK for the sabbatical support under 2223 program. Ö.D. is a member of Science Academy, Istanbul.

■ ABBREVIATIONS

LLC, lyotropic liquid crystal; QDSS, quantum-dot-sensitized solar cell; FF, fill factor; V_{oc} , open-circuit voltage; I_{sc} , short-circuit current; P25, TiO₂ nanoparticles

■ REFERENCES

- (1) Grätzel, M. Photoelectrochemical cells. *Nature* **2001**, *414*, 338–344.
- (2) Kamat, P. V.; Tvrđy, K.; Baker, D. R.; Radich, J. G. Beyond photovoltaics: semiconductor nanoarchitectures for liquid-junction solar cells. *Chem. Rev.* **2010**, *110*, 6664–6688.
- (3) Kamat, P. V. Quantum Dot Solar Cells. The next big thing in photovoltaics. *J. Phys. Chem. Lett.* **2013**, *4*, 908–918.

- (4) Hod, I.; Zaban, A. Materials and interfaces in quantum dot sensitized solar cells: challenges, advances and prospects. *Langmuir* **2014**, *30*, 7264–7273.
- (5) Baker, D. R.; Kamat, P. V. Photosensitization of TiO₂ nanostructures with CdS quantum dots. Particulates versus tubular support architectures. *Adv. Funct. Mater.* **2009**, *19*, 805–811.
- (6) Robel, I.; Subramanian, V.; Kuno, M.; Kamat, P. V. Quantum dot solar cells. Harvesting light energy with CdSe nanocrystals molecularly linked to mesoscopic TiO₂ films. *J. Am. Chem. Soc.* **2006**, *128*, 2385–2393.
- (7) Watson, D. F. Linker-assisted assembly and interfacial electron-transfer reactivity of quantum dots–substrate architectures. *J. Phys. Chem. Lett.* **2010**, *1*, 2299–2309.
- (8) Gorer, S.; Hodes, G. Quantum size effects in the study of chemical solution deposition mechanisms of semiconductor films. *J. Phys. Chem.* **1994**, *98*, 5338–5346.
- (9) Salant, A.; Shalom, M.; Hod, I.; Faust, A.; Zaban, A.; Banin, U. Quantum dot sensitized solar cells with improved efficiency prepared using electrophoretic deposition. *ACS Nano* **2010**, *4*, 5962–5968.
- (10) Santra, P. K.; Kamat, P. V. Mn-doped quantum dot sensitized solar cells: a strategy to boost efficiency over 5%. *J. Am. Chem. Soc.* **2012**, *134*, 2508–2511.
- (11) Lee, H.; Wang, M.; Chen, P.; Gamelin, D. R.; Zakeeruddin, S. M.; Grätzel, M.; Nazeeruddin, M. K. Efficient CdSe quantum dot-sensitized solar cells prepared by an improved successive ionic layer adsorption and reaction process. *Nano Lett.* **2009**, *9*, 4221–4227.
- (12) Chakrapani, V.; Baker, D.; Kamat, P. V. Understanding the role of the sulfide redox couple (S^{2-}/S_n^{2-}) in quantum dot-sensitized solar cells. *J. Am. Chem. Soc.* **2011**, *133*, 9607–9615.
- (13) Li, L.; Yang, X.; Gao, J.; Tian, H.; Zhao, J.; Hagfeldt, A.; Sun, L. Highly efficient CdS quantum dot-sensitized solar cells based on a modified polysulfide electrolyte. *J. Am. Chem. Soc.* **2011**, *133*, 8458–8460.
- (14) Jovanovski, V.; González-Pedro, V.; Giménez, S.; Azaceta, E.; Cabañero, G.; Grande, H.; Tena-Zaera, R.; Mora-Seró, I.; Bisquert, J. A Sulfide/polysulfide-based ionic Liquid electrolyte for quantum dot-sensitized solar cells. *J. Am. Chem. Soc.* **2011**, *133*, 20156–20159.
- (15) Rühle, S.; Shalom, M.; Zaban, A. Quantum-dot-sensitized solar cells. *ChemPhysChem* **2010**, *11*, 2290–2304.
- (16) Wang, J.; Mora-Seró, I.; Pan, Z.; Zhao, K.; Zhang, H.; Feng, Y.; Yang, G.; Zhong, X.; Bisquert, J. Core/shell colloidal quantum dot exciplex states for the development of highly efficient quantum-dot-sensitized solar cells. *J. Am. Chem. Soc.* **2013**, *135*, 15913–15922.
- (17) Kim, H.; Hwang, I.; Yong, K. Highly durable and efficient quantum dot-sensitized solar cells based on oligomer gel electrolytes. *ACS Appl. Mater. Interfaces* **2014**, *6*, 11245–11253.
- (18) Ma, C.; Tang, Q.; Zhao, Z.; Hou, M.; Chen, Y.; He, B.; Yu, L. Bifacial quantum dot-sensitized solar cells with transparent cobalt selenide counter electrodes. *J. Power Sources* **2015**, *278*, 183–189.
- (19) Duan, J.; Zhang, H.; Tang, Q.; He, B.; Yu, L. Recent advances in critical materials for quantum dot-sensitized solar cells: a review. *J. Mater. Chem. A* **2015**, *3*, 17497–17510.
- (20) Sharma, D.; Jha, R.; Kumar, S. Quantum dot sensitized solar cell: recent advances and future perspectives in photoanode. *Sol. Energy Mater. Sol. Cells* **2016**, *155*, 294–322.
- (21) Guijarro, N.; Campiña, J. M.; Shen, Q.; Toyoda, T.; Lana-Villarreal, T.; Gómez, R. Uncovering the role of the ZnS treatment in the performance of quantum dot sensitized solar cells. *Phys. Chem. Chem. Phys.* **2011**, *13*, 12024–12032.
- (22) O'Regan, B.; Grätzel, M. A low-cost, high-efficiency solar cell based on dye-sensitized colloidal TiO₂ films. *Nature* **1991**, *353*, 737–740.
- (23) Chiba, Y.; Islam, A.; Watanabe, Y.; Komiya, R.; Koide, N.; Han, L. Dye-sensitized solar cells with conversion efficiency of 11.1%. *Jpn. J. Appl. Phys., Part 2* **2006**, *45*, L638–L640.
- (24) Hagfeldt, A.; Boschloo, G.; Sun, L.; Kloo, L.; Pettersson, H. Dye-sensitized solar cells. *Chem. Rev.* **2010**, *110*, 6595–6663.
- (25) Karakaya, C.; Türker, Y.; Dag, Ö. Molten-salt-assisted self-assembly (MASA)-synthesis of mesoporous metal titanate-titania, metal sulfide-titania, and metal selenide-titania thin films. *Adv. Funct. Mater.* **2013**, *23*, 4002–4010.
- (26) Karakaya, C.; Türker, Y.; Albayrak, C.; Dag, Ö. Assembly of molten transition metal salt–surfactant in a confined space for the synthesis of mesoporous metal oxide-rich metal oxide–silica thin films. *Chem. Mater.* **2011**, *23*, 3062–3071.
- (27) Avci, C.; Aydın, A.; Tuna, Z.; Yavuz, Z.; Yamauchi, Y.; Suzuki, N.; Dag, Ö. Molten salt assisted self assembly (MASA): synthesis of mesoporous metal titanate (CoTiO₃, MnTiO₃, and Li₄Ti₅O₁₂) thin films and monoliths. *Chem. Mater.* **2014**, *26*, 6050–6057.
- (28) Brinker, C. J.; Lu, Y.; Sellinger, A.; Fan, H. Evaporation-induced self-assembly: nanostructures made easy. *Adv. Mater.* **1999**, *11*, 579–585.
- (29) Türker, Y.; Karakaya, C.; Dag, Ö. Fabrication of mesoporous metal chalcogenide nanoflake silica thin films and spongy mesoporous CdS and CdSe. *Chem.—Eur. J.* **2012**, *18*, 3695–3705.
- (30) Rodrigues, L. C. V.; Brito, H. F.; Hölsä, J.; Stefani, R.; Felinto, M. C. F. C.; Lastusaari, M.; Laamanen, T.; Nunes, L. A. O. Discovery of the persistent luminescence mechanism of CdSiO₃:Tb³⁺. *J. Phys. Chem. C* **2012**, *116*, 11232–11240.
- (31) Engelhardt, G.; Michel, D. *High-Resolution Solid-State NMR of Silicates and Zeolites*; Wiley: New York, 1987; pp 77–135.
- (32) Tobaldi, D. M.; Pullar, R. C.; Seabra, M. P.; Labrincha, J. A. Fully quantitative x-ray characterisation of Evonik aerioxide TiO₂ P25. *Mater. Lett.* **2014**, *122*, 345–347.
- (33) Ptatschek, V.; Schreder, B.; Herz, K.; Hilbert, U.; Ossau, W.; Schottner, G.; Rahäuser, O.; Bischof, T.; Lermann, G.; Materny, A.; Kiefer, W.; Bacher, G.; Forchel, A.; Su, D.; Giersig, M.; Müller, G.; Spanhel, L. Sol–gel synthesis and spectroscopic properties of thick nanocrystalline CdSe films. *J. Phys. Chem. B* **1997**, *101*, 8898–8906.
- (34) Yannopoulos, S. N.; Andrikopoulos, K. S. Raman scattering study on structural and dynamical features of nanocrystalline selenium. *J. Chem. Phys.* **2004**, *121*, 4747–4758.
- (35) Alivisatos, A. P.; Harris, T. D.; Carroll, P. J.; Steigerwald, M. L.; Brus, L. E. Electron–vibration coupling in semiconductor clusters studied by resonance Raman spectroscopy. *J. Chem. Phys.* **1989**, *90*, 3463–3468.
- (36) Zhang, W. F.; He, Y. L.; Zhang, M. S.; Yin, Z.; Chen, Q. Raman scattering study on anatase TiO₂ nanocrystals. *J. Phys. D: Appl. Phys.* **2000**, *33*, 912–916.